Virology 531 (2019) 126–140

Contents lists available at ScienceDirect

Virology

journal homepage: www.elsevier.com/locate/virology

Local structural changes of the influenza A virus ribonucleoprotein complex by single mutations in the specific residues involved in efficient genome packaging

Naoki Takizawa[a,*], Yoshitoshi Ogura[b], Yoko Fujita[c,d], Takeshi Noda[c,d], Hideki Shigematsu[e], Tetsuya Hayashi[b], Ken Kurokawa[f]

[a] Laboratory of Virology, Institute of Microbial Chemistry (BIKAKEN), Tokyo, Japan
[b] Department of Bacteriology, Faculty of Medical Sciences, Kyushu University, Fukuoka, Japan
[c] Laboratory of Ultrastructural Virology, Institute for Frontier Life and Medical Sciences, Kyoto University, Kyoto, Japan
[d] Laboratory of Ultrastructural Virology, Division of Integrated Life Science, Graduate School of Biostudies, Kyoto University, Kyoto, Japan
[e] Life Science Research Infrastructure Group, RIKEN SPring-8 Center, Hyogo, Japan
[f] Center for Information Biology, National Institute of Genetics, Shizuoka, Japan

ARTICLE INFO

Keywords:
Influenza virus
Genome packaging
VRNP structure
RNA structure

ABSTRACT

The influenza A virus genome consists of eight single-stranded negative-sense RNA segments. The noncoding regions located at the 3′- and 5′- ends of each segment are necessary for genome packaging, and the terminal coding regions are required to precisely bundle the eight segments. However, the nucleotide residues important for genome bundling are not defined. Here, we introduced premature termination codons in the hemagglutinin (HA) or matrix protein 2 (M2) gene and constructed virus libraries containing random sequences in the terminal coding regions. Using these virus libraries, we identified nucleotide residues involved in efficient virus propagation. Viral genome packaging was impaired in viruses that contained single mutations at these identified residues. Furthermore, these single mutations altered the local structure of the viral ribonucleoprotein complex. Our results show that specific nucleotide residues in the viral protein coding region are involved in forming the precise structure of the viral ribonucleoprotein complex.

1. Introduction

The influenza A virus is a member of the *Orthomyxoviridae* family and is characterized by a segmented genome that consists of eight single-stranded negative-sense viral RNA (vRNA) segments. The vRNA is complexed with a heterotrimeric viral RNA polymerase complex and nucleoproteins (NP) to form a viral ribonucleoprotein complex (vRNP). Each infectious virion must contain a full set of eight segments. Recent studies favor the “selective packaging” model, in which one set of the eight distinct vRNAs is selectively incorporated into progeny virions (Noda et al., 2006; Chou et al., 2012). The 12 nucleotides at the 3′ termini and the 13 nucleotides at the 5′ termini of the vRNAs are highly conserved between segments. These 3′ and 5′ conserved sequences are partially complementary and anneal to form a hairpin structure necessary for viral RNA synthesis. These sequences are also essential for the incorporation of vRNPs into a budding viral particle (Giese et al., 2016).

Other sequences required for efficient viral genome packaging have been identified in each of the eight segments (Gerber et al., 2014). These sequences, so-called segment-specific packaging signals, are located in both of the terminal noncoding and coding regions at the 3′ and 5′ ends of each vRNA segment. Deletions or mutations in the segment-specific packaging signals reduce the packaging efficiency not only of the mutated vRNA segment but also that of the other vRNA segments into the virion (Zhao et al., 2014; Hutchinson et al., 2008, 2009; Marsh et al., 2007, 2008; Muramoto et al., 2006). Goto et al. reported that the terminal coding regions of each segment-specific packaging signal are required for the packaging of one set of eight segments and proposed that those in the 3′ and 5′ noncoding regions, named incorporation signals, are essential for genome packaging and that those in the terminal coding regions, named bundling signal (BS), are necessary for bundling the eight segments (Goto et al., 2013). Whether the regions and nucleotide residues involved in segment bundling are distinguishable from those involved in the genome packaging is not known. The

* Corresponding author.
E-mail address: takizawan@bikaken.or.jp (N. Takizawa).

https://doi.org/10.1016/j.virol.2019.03.004
Received 7 December 2018; Received in revised form 5 March 2019; Accepted 6 March 2019
Available online 07 March 2019
0042-6822/

eight segments are assumed to be bundled by direct RNA-RNA interactions between segments, because vRNAs can form specific networks of intermolecular interactions *in vitro* (Gilbertson et al., 2016; Gavazzi et al., 2013a, 2013b; Fournier et al., 2012) and an RNA-RNA interaction between segments is required for efficient viral genome packaging (Gavazzi et al., 2013a). Recent studies have shown that NP does not bind vRNA uniformly and NP enriched or poor sites exist in each vRNA segment (Lee et al., 2017; Williams et al., 2018), suggesting that vRNPs can form RNA interactions and specific RNA structures. In addition, direct contact between vRNPs has been observed in electron tomography of purified viral particles (Noda et al., 2012). However, the precise roles of BSs are currently unknown.

The replication of the influenza viral genome and transcription of viral mRNA occur in the nucleus of infected cells. Newly synthesized vRNPs are exported from the nucleus to the cytoplasm *via* a CRM1-dependent pathway, in which two viral proteins, M1 and NEP, are involved (Hutchinson and Fodor, 2013). After export from the nucleus, vRNPs accumulate in the perinuclear region and associate with the endosomal recycling compartment. The vRNPs are then transported to the apical plasma membrane through interaction with Rab11-positive vesicles (Eisfeld et al., 2011; Momose et al., 2011; Amorim et al., 2011). Multiple vRNA segments are bundled in the cytoplasm as single-molecule sensitivity FISH analysis showed that the different segments co-localized with Rab11 (Chou et al., 2013; Lakdawala et al., 2014; Takizawa et al., 2010). These reports support a model in which all eight vRNA segments are bundled together on Rab11-positive vesicles *en route* to the apical plasma membrane and Rab11-positive vesicles serve as a platform for viral genome bundling.

Identification of nucleotide residues important for genome packaging and bundling has been attempted by introducing synonymous mutations in the segment-specific signal sequence regions (Hutchinson et al., 2008, 2009; Marsh et al., 2007, 2008; Gog et al., 2007). Gog et al. identified codons showing little synonymous variation in a large data set of reported influenza virus sequences and showed that synonymous mutations in these codons reduced segment packaging (Gog et al., 2007). Although such an approach to introduce synonymous mutations into the BSs provided valuable information for the elucidation of molecular mechanisms of genome bundling, a more systematic identification of nucleotide residues involved in the segment bundling is difficult, because the signal sequences exist in the terminal coding regions of each segment. Here, to overcome these limitations, we utilized recombinant viruses that did not express HA or M2 proteins by introducing premature termination codons and cells expressing HA or M2 to complement these lacking viral proteins. To identify the specific residues involved in genome bundling and packaging, we constructed recombinant virus libraries, in which each mutant virus contained premature termination codons and random sequences in the BS. Using these recombinant virus libraries and cells expressing HA or M2, *cis*-acting nucleotide residues required for efficient genome packaging were identified. We also found that the local structures of vRNP containing single mutations at the identified residues are altered around the mutation sites. Our results suggest that specific nucleotide residues have important roles in the formation of a precise vRNP structure for efficient genome packaging.

2. Materials and methods

2.1. Vectors and antibodies

The oligonucleotide sequences of primers used in this study are listed in Table S1. Viral protein expression vectors and viral RNA expression vectors derived from strain A/WSN/33 were kindly provided by Dr. Y. Kawaoka (Neumann et al., 1999). To construct pPolI-WSN-M2stop, inverted PCR was carried out using pPolI-WSN-M (Neumann et al., 1999) as a template with specific primer sets. In pPolI-WSN-HAstop (Takizawa et al., 2016) and pPolI-WSN-M2stop, premature termination codons were introduced at lysine 4 and leucine 5 in HA and at proline 25 and leucine 26 in M2. To construct pPolI-WSN-HAstop1656N, 1676N, 1687N, 1698N, 1708N, and 1718N, and pPolI-WSN-M2stop960N, 972N, 984N, and 996N, inverted PCR was carried out using pPolI-WSN-HAstop or pPolI-WSN-M2stop as a template with specific primer sets with a random sequence at the 5′ end. After *Dpn*I treatment, phosphorylation, ligation, and transformation into *Escherichia coli* Mach1 (Thermo Fisher Scientific, Waltham, MA), all colonies (approximately 50,000) were collected to create plasmid libraries. After purification of these plasmids, inverted PCR was carried out again using the same primer sets to reduce the proportion of plasmids containing wild type sequences. To prevent trypsin-independent cleavage of WSN virus HA, pPolI-WSN-NA R130N was used to generate recombinant viruses and WSN NA R130N virus was used as the wild type virus (Takizawa et al., 2016).

Rabbit polyclonal antibodies against NP and M1 were kindly provided by Dr. K. Nagata (Kawaguchi et al., 2011) and Dr. K. Kobayashi (Takizawa et al., 2006), respectively. Rabbit polyclonal antibody against FLAG tag was purchased from MBL (Nagoya, Japan). Mouse monoclonal antibody RA5-22 against HA was provided by BEI Resources, NIAID, NIH (Bethesda, MD), and mouse monoclonal antibody C179 against HA was purchased from Takara Bio Inc. (Otsu, Japan). A sheep polyclonal antibody against NA was purchased from R&D Systems (Minneapolis, MN). Mouse monoclonal antibody mAb61A5 against NP was kindly provided by Dr. F. Momose (Momose et al., 2007).

2.2. Cells

HEK293T cells (kindly provided by Dr. Y. Kawaoka) and MDCK cells expressing FLAG-Rab11 (MDCK-F11-WT) (Momose et al., 2011) were maintained in Dulbecco's modified Eagle's medium (DMEM) with high glucose (Sigma-Aldrich, ST. Louis, MO) containing 10% fetal bovine serum and penicillin/streptomycin (Nacalai Tesque, Kyoto, Japan). MDCK cells (American Type Culture Collection, Manassas, VA) and MDCK expressing HA (MDCK-HA) cells (Takizawa et al., 2016) were maintained in minimal essential medium (MEM) (Wako Pure Chemical Industries, Osaka, Japan) containing 10% fetal bovine serum and penicillin/streptomycin. To establish MDCK cells expressing M2 (MDCK-M2), MDCK cells were transfected with pCAGGS-M2 (Neumann et al., 1999) and pCI-neo (Promega, Fitchburg, WI). The transfected cells were selected under 500 μg/ml G418 (Nacalai Tesque) and G418-resistant cell foci were picked after 1 week of selection. MDCK-M2 cells were maintained in MEM containing 10% fetal bovine serum and penicillin/streptomycin.

2.3. Recombinant virus and virus library construction

Recombinant viruses and virus libraries were generated using a reverse genetics approach (Neumann et al., 1999). HEK293T cells were transfected with viral protein and viral RNA expression vectors using polyethylenimine (Polysciences, Warrington, PA). After 24 h of transfection, the culture medium was changed to OPTI-MEM I (Life-Technologies, Gaithersburg, MD) containing 0.6 μg/ml TPCK-trypsin (Sigma-Aldrich). After incubation for 24 h, the cell culture supernatant was collected, and the virus titer was determined by plaque assay using MDCK-HA or MDCK-M2. Recombinant viruses were propagated using MDCK-HA or MDCK-M2 cells and used for infection assays.

2.4. Targeted amplicon sequencing

The selection of virus libraries was performed by virus passage. MDCK-HA or MDCK-M2 cells were infected with the virus libraries at a multiplicity of infection (MOI) of 0.05. At 48 h post infection (hpi), the supernatants were collected and used for the next infection. The virus libraries at passages 1, 3, and 5 were used to infect MDCK-HA or MDCK-

M2 cells. Total RNA was extracted using ISOGEN reagent (Nippon Gene, Tokyo, Japan) at 8 hpi and cDNA was synthesized with the Uni12 primer using ReverTra Ace (Toyobo, Osaka, Japan). The fragments of segment 4 (nucleotide positions 1570–1764) or segment 7 (nucleotide position 738–1027) were amplified with specific primers using the KAPA HiFi HS ReadyMix (Kapa Biosystems, Wilmington, MA). A second PCR to construct a sequencing library was performed with the Nextera XT Index Primers (Illumina, San Diego, CA) using KAPA HiFi HS ReadyMix. Sequencing was performed using a MiSeq sequencer (Illumina) with MiSeq Reagent Kit v3 (600 cycles) (Illumina). The sequence data have been deposited into DDBJ Sequence Read Archive (DRA Accession: DRA003947 and DRA005679).

2.5. Data analysis

Read sequences were filtered according to base quality using the FASTQ Quality Filter (q = 20). The 6- or 7-nucleotide sequences that flanked the random sequence-inserted region were identified in each read and the sequences between the flanking sequences were extracted. Matched fragments in the paired-reads were used for the following analysis. Using the AWK script, sequences were extracted and counted, and the ratio of nucleotides in each position and the Hamming distances were calculated. Duplicate fragments were removed when the Hamming distance was calculated.

2.6. Western blotting and RT-qPCR assay

MDCK-M2 cells were infected with recombinant virus at an MOI of 1, and the cells were suspended in MEM. At 24 hpi, the supernatant was collected, and cell debris was removed by low speed centrifugation (500 × *g*, 5 min) and filtration through a 0.45-μm filter (EMD Millipore, Billerica, MA). The pre-cleared supernatant was layered on a buffer containing 20 mM Tris-HCl (pH 7.9), 100 mM NaCl, 1 mM EDTA, and 30% sucrose and centrifuged at 130,000 × *g* for 1.5 h using an SW55 rotor (Beckman Coulter, Brea, CA). The pellet was suspended in 100 μl of PBS(-). An *in vitro* synthesized yeast Cet1 RNA fragment (10 ng) was added as an RNA spike-in control of the RT-qPCR assay.

MDCK-M2 cells were infected with the recombinant virus at an MOI of 1 in MEM, and the infected cells were collected at 8 hpi. The infected cells were suspended in lysis buffer (20 mM Tris-HCl [pH 7.9], 150 mM NaCl, 1 mM EDTA, and 0.1% NP-40), and the protein concentration was determined using Protein Assay Reagent (Bio-Rad, Hercules, CA). Part of the lysate was collected for western blotting and the total RNA was extracted from the lysate using ISOGEN reagent (Nippon Gene). The lipid raft fraction was prepared as described previously (Takizawa et al., 2016).

Viral proteins in the virions and cell lysate were separated by SDS-PAGE and detected by western blotting using an ImageQuant LAS 4000 (GE Healthcare, Milwaukee, WI). NP and M1 were detected using rabbit polyclonal antibodies and HA was detected using mouse monoclonal antibody RA5-22. Band intensities were measured using ImageJ software (Schneider et al., 2012), and standard curves were generated to semi-quantify the relative amount of viral proteins.

For RT-qPCR, cDNA was synthesized with Uni12 and 18S rRNA-specific primers for total RNA or Cet1-specific primer for viral RNA using ReverTra Ace (Toyobo). The synthesized cDNA was mixed with Thunderbird SYBR qPCR mix (Toyobo) and a specific primer set for each segment. The qPCR reactions were performed using a Thermal Cycler Dice Real Time System TP800 (Takara Bio), and the relative amounts of each segment were calculated.

2.7. Hemaggulutination assay

A hemagglutination (HA) assay was performed with 0.5% chicken red blood cells (NIPPON BIO-TEST LABORATORIES, Saitama, Japan) at 25°C using a standard method (World Health Organization, 2011). The HA titers of viruses were determined by the average from four independent experiments of the same sample.

2.8. Electron microscopy

MDCK-M2 cells were infected with recombinant virus at an MOI of 0.01, and the supernatant was collected at 48 hpi. After removal of cell debris by low speed centrifugation (500 × *g*, 5 min) and filtration through a 0.45-μm filter, the supernatant was layered onto a 30% sucrose/PBS cushion, and ultracentrifuged at 100,000 × *g* for 1.5 h using an SW28 rotor (Beckman Coulter). The pellet was suspended in PBS(-), negatively stained with 2% phosphotungstic acid, and observed by transmission electron microscopy (Hitachi HT-7700) at 80 kV. The virus particles were counted using the ImageJ software.

2.9. Indirect immunofluorescence

An indirect immunofluorescence assay was performed as described previously (Takizawa et al., 2016). Mouse anti-HA monoclonal antibody C179, sheep anti-NA polyclonal antibody, and rabbit anti-M1 polyclonal antibody were used to immunostain viral proteins. Alexa Fluor 594-conjugated anti-rabbit IgG (Thermo Fisher Scientific), Alexa Fluor 488-conjugated anti-sheep IgG (Thermo Fisher Scientific), Alexa Fluor 594-conjugated anti-mouse IgG (Thermo Fisher Scientific), and Alexa Fluor 488-conjugated anti-mouse IgG (Thermo Fisher Scientific) were used for visualization. Specimens were observed under a DMI6000 B microscope (Leica Microsystems, Wetzlar, Germany) or an LSM 5 confocal microscope (Carl Zeiss, Jena, Germany).

2.10. Dimethyl sulfate (DMS) and 2-methylnicotinic acid imidazolide (NAI) labeling

DMS was purchased from Wako Pure Chemical Industries, and NAI was synthesized as described previously (Spitale et al., 2013). Briefly, 1 mmol of 2-methylnicotinic acid (Sigma-Aldrich) was dissolved in 0.5 ml of anhydrous DMSO (Wako Pure Chemical Industries). One mmol of 1,1′-carbonyldiimidazole in 0.5 ml of anhydrous DMSO was added dropwise to the solution over 5 min. The resulting solution was stirred at 25°C until gas evolution was complete and then stirred at 25°C for an additional 1 h using a ThermoMixer C (Eppendorf, Hamburg, Germany). The resulting solution was used as a 1 M stock solution containing a 1:1 mixture of NAI and imidazole.

MDCK-M2 cells were infected with the recombinant virus at an MOI of 0.01, and the cells were suspended in MEM containing 0.6 μg/ml TPCK-trypsin. At 24 hpi, the virus in the supernatant was pelleted as described above, and the pellet was resuspended in 100 μl of the DMS buffer (40 mM Hepes-NaOH, 100 mM NaCl, and 0.5 mM $MgCl_2$), and 1 μl of DMS or 5 μl of NAI was added. After incubation for 15 min (DMS) or 45 min (NAI) at 25°C, 10 μl of 1 M DTT was added to stop the reaction. Then, viral RNA was extracted with phenol/chloroform. The ^{32}P-labelled oligonucleotide specific to segment 7 (Seg7v 107) was mixed, and primer extension was performed using ReverTra Ace (Toyobo). The products were separated by 6% UREA-PAGE and visualized using a Typhoon 9400 image analyzer (GE Healthcare). To synthesize control RNA, segment 7 cDNA with a T7 promoter was amplified from pPolI-WSN-M using specific primers, and segment 7 vRNA was synthesized using T7 RNA polymerase (Takara Bio). To determine the reverse-transcription stop position, primer extension was performed with 0.5 mM ddATP, ddGTP, ddTTP, or ddCTP (Sigma-Aldrich) using *in vitro* synthesized segment 7 vRNA fragment as a template.

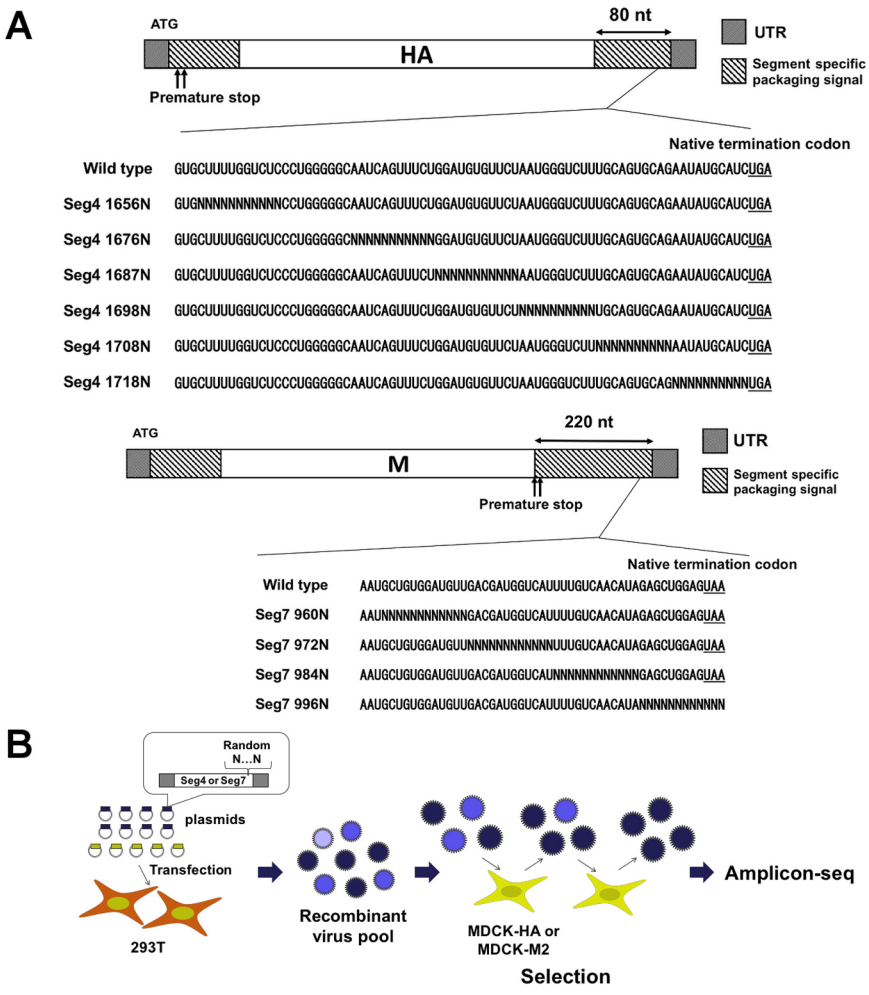

Fig. 1. Schematic representation of the method for the screening of the virus libraries. (A) The recombinant virus libraries containing random sequences. Premature termination codons were introduced to stop viral protein synthesis, and a sequence of 10 – 12 random nucleotides was introduced into the bundling signal of segment 4 or segment 7. The native termination codons are underlined. The virus libraries were constructed using a reverse genetics system. (B) Selection of the virus libraries. The virus library was passaged in MDCK-HA or MDCK-M2 cells to complement the lack of HA or M2 expression from the viral mRNA. All nucleotide sequences are shown in the positive-sense orientation.

3. Results

3.1. Selection of the virus libraries in which each clone contains a random sequence in the BS

The large limitation to identifying the nucleotide residues important for genome bundling or packaging in a BS is that nonsynonymous mutations are not permitted. To overcome the limitation, we constructed a new system utilizing recombinant viruses containing premature termination codons in segment 4 or 7 to terminate translation of HA or M2 from viral mRNA (HAstop virus and M2stop virus, respectively) and MDCK cells expressing HA or M2 to complement the lack of these viral proteins (Fig. 1A). We constructed the HAstop and M2stop virus-derived libraries, in which each clone contained a sequence of 10 – 12 random nucleotides at the 3′ end of the 3′ BS in the positive-sense orientation. The reported lengths of the BSs of segments 4 and 7 in the 3′ region are 80 and 220 nucleotides, respectively (Marsh et al., 2007; Ozawa et al., 2009). The selection of preferentially propagating viruses in the library was performed by passaging of the virus library in MDCK-HA or MDCK-M2 cells (Fig. 1B). In this system, random sequences did not affect viral protein synthesis; thus, we could identify the nucleotide residues required for efficient virus propagation without considering the effects of amino acid sequence changes in HA and M2. We constructed six HA stop virus-derived libraries, each containing a random sequence in nucleotide positions 1656 – 1666 (1656N), 1676 – 1686 (1676N), 1687 – 1697 (1687N), 1698 – 1707 (1698N), 1708 – 1717 (1708N), or 1718 – 27 (1718N) in segment 4 (a virus library containing a random sequence in positions 1667 – 1675 was missing because the library plasmid could not be amplified), and four M2stop virus-derived libraries, each containing a random sequence in nucleotide positions 960 – 971 (960N), 972 – 983 (972N), 984 – 995 (984N), or 996 – 1007 (996N) in segment 7. Approximately 19,000–64,000 kinds of introduced random sequences were confirmed in each plasmid library used for construction of the virus library (S1 File). Approximately 69 – 89% of the plasmids in each library contained the correct length of nucleotides in the mutated region.

MDCK-HA or MDCK-M2 cells were infected with each virus library and passaged five times. To determine the sequences that were selected by this screening, total RNA was extracted from the cells infected with the virus libraries that were passaged one, three, or five times, and a large-scale sequencing analysis was performed using the Amplicon-seq method. The obtained sequences were aligned, and the numbers of each sequence appearing in the random sequence-introduced region were counted. The total number of reads and that of the aligned reads in each sample are listed in Table S2. The top five sequences appearing in each library at passage 5 and their ratios to the total aligned reads are shown in Fig. 2. The list of all counted sequences that appeared in each library at passage 1, 3, 5, and that of the parental plasmids are shown in the S1 File. The ratios of these selected sequences to the total aligned reads increased from passage 1–5 in all virus libraries, suggesting that the viruses containing sequences preferable for efficient virus propagation were enriched by passaging. At passage 5, the wild-type sequence was not ranked as the top sequence in any virus libraries, except for segment 4 1676N and segment 7 960N. The ratio of the top 20 sequences of plasmids used to prepare each virus library are shown in Table S3. Except for segment 4 1676N, the sequences ranked as top sequences at passage 5 in each virus library were not enriched in parental plasmids, suggesting that the sequences preferable for efficient virus propagation

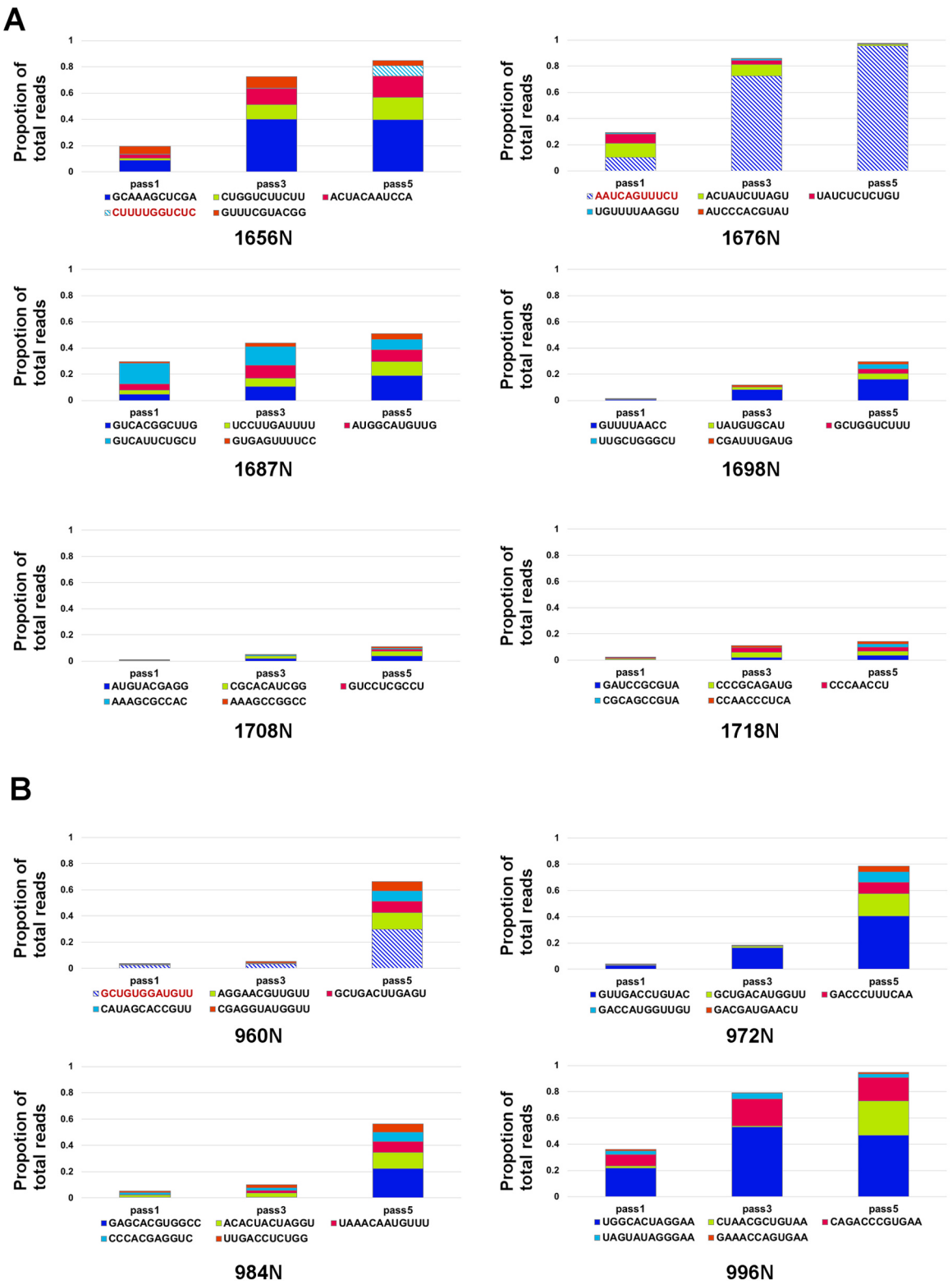

Fig. 2. Sequences selected by screening and the enrichment of these sequences through passaging. The top five sequences appearing after passage 5 in each of the six virus libraries for segment 4 (A) and of the four virus libraries for segment 7 (B) were analyzed. The proportions of each sequence among the total number of sequences after passage 1, 3, and 5 for each library are shown. Wild-type sequences are presented with a diagonal bar and indicated in red in the graph legend.

were enriched after passaging. These results suggest that the sequences in a BS can vary without impairing the efficiency of virus propagation if there is no restriction of translation by providing the wild type gene products (HA or M2) *in trans*.

To confirm that the enrichment of sequences did not occur as a result of a PCR bias of the Amplicon-seq method or other technical reasons but was due to the selective enrichment of viruses containing sequences preferable for efficient virus propagation, we analyzed whether sequences similar to the most enriched sequence after 5 passages were also enriched. To analyze this, the number of positions at

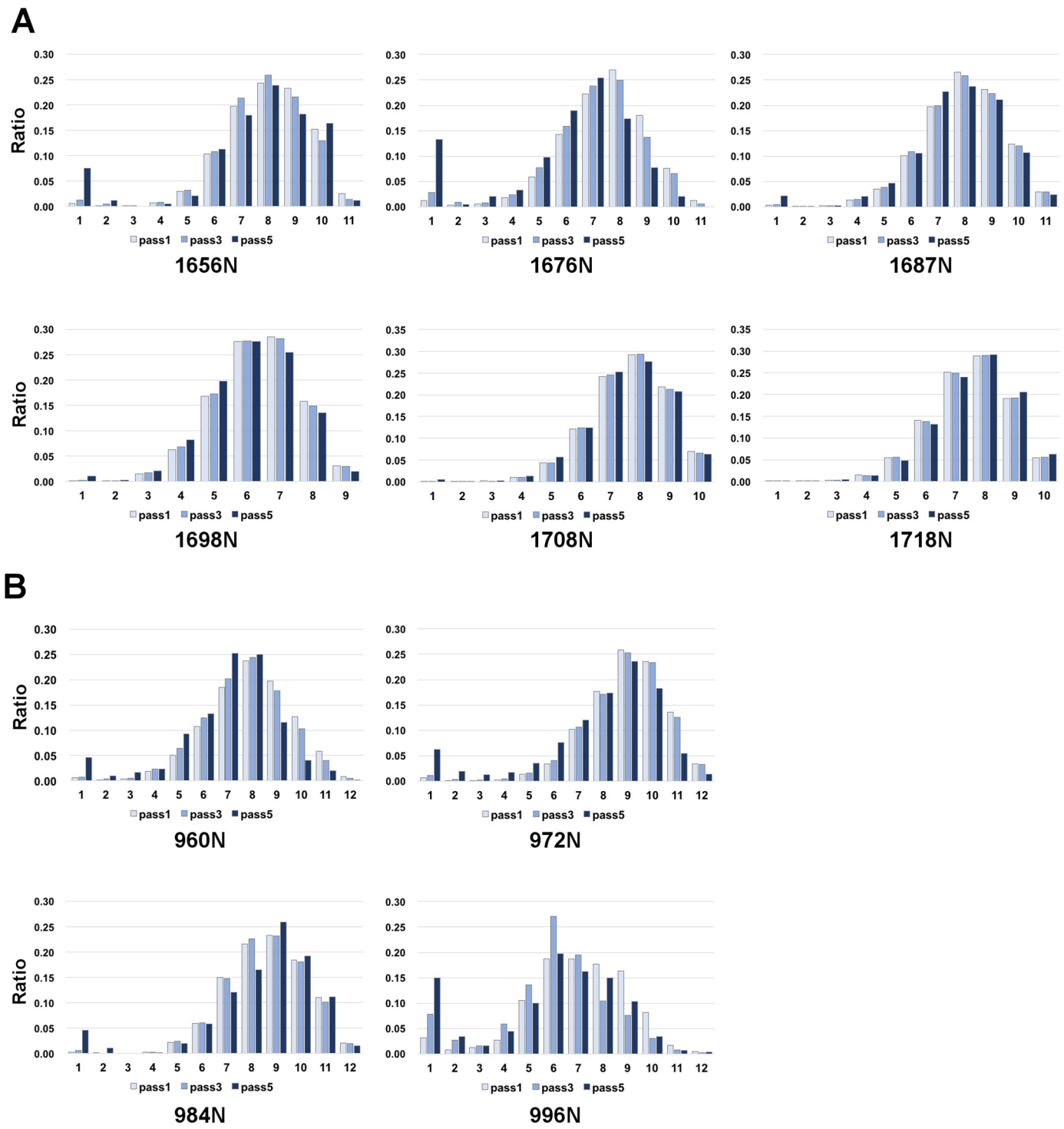

Fig. 3. Ratios of sequences with each Hamming distance between the most enriched sequence after passage 5 and each sequence appearing in the random sequence-introduced region. The Hamming distance between each sequence appearing in the random sequence-introduced region and most enriched sequence of each library for segment 4 (A) and segment 7 (B) after 5 passages was calculated. The graph shows the ratio of the sequences with each Hamming distance.

which bases were different (the Hamming distances) between each sequence appearing in the random sequence-introduced region and the most enriched sequence after 5 passages in each virus library was calculated. If the viruses containing sequences similar to the most enriched sequence were enriched after passaging, the ratio of sequences having Hamming distances would increase. To calculate Hamming distance, duplicate fragments and longer and shorter fragments were removed from the dataset. The ratios of sequences having each Hamming distance between the most enriched sequence at passage 5 and each sequence appearing in the random sequence-introduced region at passage 1, 3, and 5 are shown in Fig. 3. Among the HAstop virus-derived libraries, the ratio of sequences with a Hamming distance of 1 increased after 5 passages in the 1656N and 1676N libraries and slightly increased in the 1687N and 1698N libraries, whereas no increase was observed in the 1708N and 1718N libraries (Fig. 3A). Among the M2stop virus-derived libraries, the ratio of sequences with Hamming distances of 1 and 2 increased after 5 passages in all libraries (Fig. 3B). These results indicate that the viruses containing the sequences similar

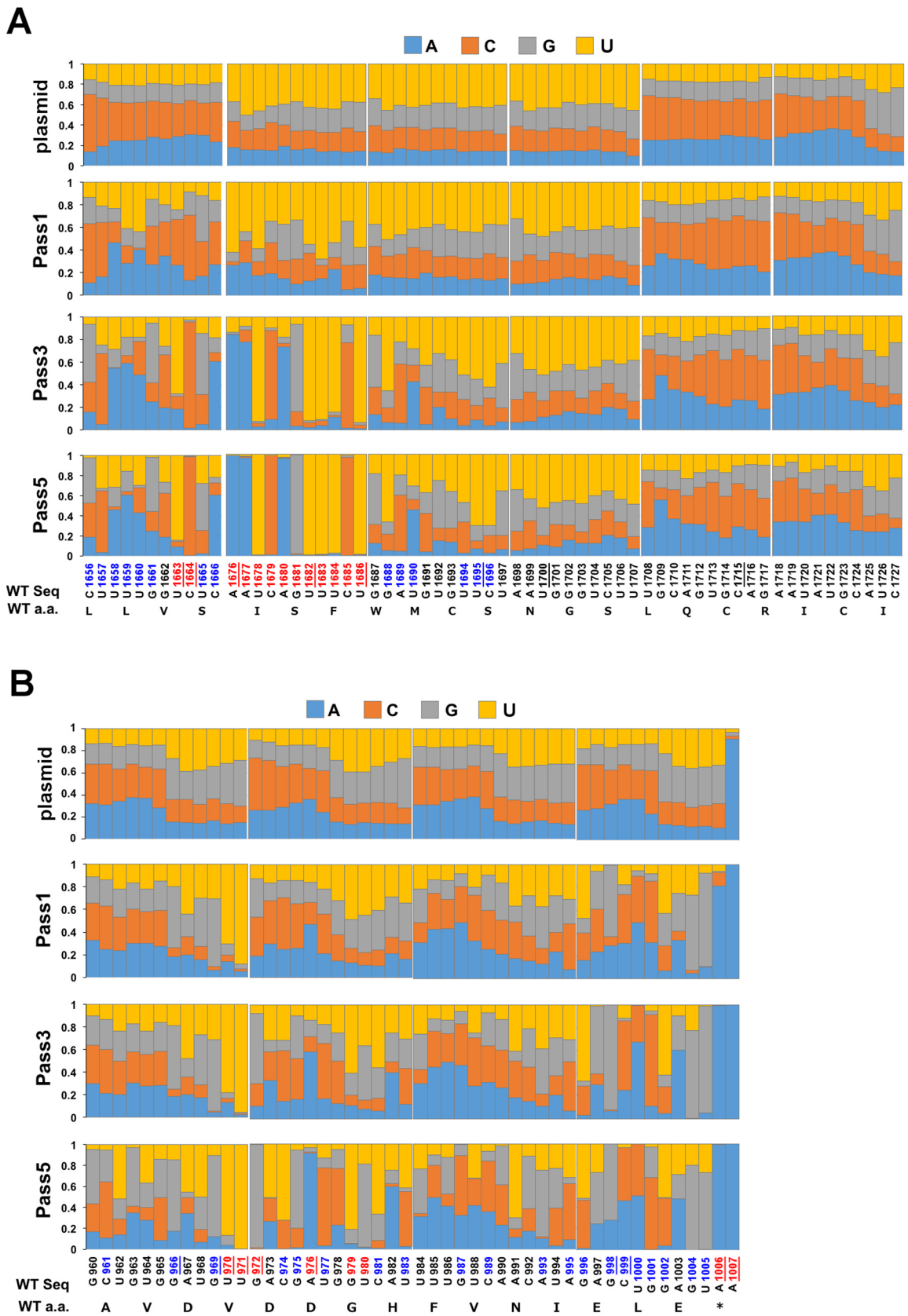

Fig. 4. Ratio of nucleotides in the sequence appearing in the random sequence-introduced region in the passaged virus libraries. The ratio of each nucleotide in the sequence appearing in the random sequence-introduced region in the virus libraries was calculated. The ratios of nucleotides at each position in segment 4 (A) and segment 7 (B) plasmid libraries and virus libraries after passage 1, 3, and 5 are shown. The nucleotide numbers and wild-type sequence are shown under the graph. The wild-type amino acid sequences are also shown to indicate the third codon positions. All nucleotide sequences and numbers are shown in the positive-sense orientation. Red nucleotide positions are a group in which the specific nucleotides were enriched through passaging. Blue nucleotide positions are a group in which the ratios of the four nucleotides were altered from passage 1–5 (A) or two nucleotides were enriched (B). The underline indicates nucleotide positions selected for the subsequent recombinant virus assay.

to the most enriched sequence after 5 passages were also enriched in segment 4 1656N, 1676N, 1687N, and 1698N libraries and all segment 7 libraries, supporting the notion that the viruses containing preferable sequences for efficient virus propagation were enriched in these libraries. In segment 4 1708N and 1718N libraries, the viruses containing specific sequences were not well enriched after 5 passages, and thus, the ratio of sequences with a Hamming distance of 1 did not increase (Figs. 2A and 3A).

3.2. Identification of the nucleotide residues required for efficient virus production

To identify the nucleotide residues required for efficient virus production, the ratios of four nucleotides at each position in all aligned sequences were calculated. The ratios of each nucleotide in each introduced random sequence at passages 1, 3, and 5 and those in the plasmid libraries used to prepare the virus libraries are shown in Fig. 4. In the result of virus passage of segment 4 virus libraries, the alteration of the ratios of the four nucleotides at each nucleotide position were categorized in three groups in which the specific nucleotides were enriched (more than 80% of total nucleotides) through passages (red nucleotide positions in Fig. 4A), the ratios of the four nucleotides were altered from passage 1 to passage 5 (blue nucleotide positions in Fig. 4A), and the ratios of the four nucleotides were almost the same at passages 1, 3, and 5 (other positions) (Fig. 4A). Specific nucleotides were enriched in nucleotide positions from 1676 to 1686 because the wild-type sequence was highly enriched after passage in the segment 4 1676N library (Figs. 2A and 4A). In the result of virus passage of segment 7 virus libraries, the alteration of the ratios of the four nucleotides were categorized in three groups in which the specific nucleotides were enriched (red nucleotide positions in Fig. 4B), two nucleotides were enriched (blue nucleotide positions in Fig. 4B), or the ratios of the four nucleotides were slightly altered or almost the same (other positions) (Fig. 4B). We selected nucleotide residues in which specific nucleotides were enriched (U1663 and U1664), three nucleotide residues located from 1676 to 1686 (A1676, U1682, and U1686), and one or two nucleotide residues in the other group (U1695, U1700, and C1715) in segment 4 and nucleotide residues in which specific nucleotides were highly enriched (more than 90%; U970, U971, G972, A976, A1006, and A1007) and four nucleotide residues in two nucleotide residues enriched group (G966, G969, G998, and C999) in segment 7. To test whether the identified nucleotide residues play a role in virus propagation, recombinant HAstop or M2stop viruses, each having a single mutation at each position selected, were constructed and the propagation of the mutant viruses was analyzed. A single mutation was introduced at each position from wild-type nucleotides to the lowest frequency nucleotide after passage 5. The mutant M2stop virus containing the A1007G mutation could not be constructed in our reverse genetics system for unknown reason(s). The MDCK-HA cells were infected with mutant viruses and parental HAstop virus at an MOI of 0.01 and MDCK-M2 cells were infected with mutant viruses and parental M2stop virus at an MOI of 0.001 because the titers of M2stop virus and mutant viruses from transfection supernatant of 293T cells were low (approximately $1-2\times10^4$ PFU/ml). The supernatants were collected at 24 hpi, and the virus titers in the supernatants were determined by plaque assay. *P*-values were calculated by the Student's *t*-test and the Benjamini-Hochberg multiple-test correction method. The propagation of all viruses containing a single mutation at the selected eight selected positions in segment 4 was comparable to that of the parent HAstop virus (Fig. 5A). The propagation of viruses containing the single mutations of U971C, C999G, or A1006G in segment 7 was reduced compared to that of the M2stop virus (Fig. 5B; corrected *P*-values were 0.148, 0.104, and 0.104, respectively). Next, propagation of the mutant viruses was assessed and compared to that of the M2stop virus. The maximum titers of these mutant viruses were still slightly lower than that of M2stop virus (Fig. 5C). To analyze whether the introduced single mutations are maintained after multiple replication cycles, the sequence of segment 7 after multicycle replications was determined. Viral RNA was purified from the supernatant that was collected at 48 hpi from cells infected at an MOI of 0.001. Fig. 5D shows the obtained sequences around the mutation sites. The single mutations were maintained after multicycle replication (Fig. 5D, underline). These results suggest that nucleotide residues at these three positions in segment 7 play an important role in efficient virus propagation.

3.3. Impairment of viral genome packaging by single mutations at positions U971, C999, and A1006 in segment 7 of M2stop virus

To determine which step of virus propagation is impaired by single mutations at positions U971, C999, and A1006 in segment 7, the amounts of viral proteins and vRNA in infected cells were determined. The amounts of HA, NP, and M1 in the cells infected with the virus containing the U971C, C999G, or A1006G mutation at 8 hpi were comparable to those in cells infected with the M2stop virus (Fig. 6A and B). The amounts of vRNA segments in the mutant virus-infected cells were also comparable to those in the M2stop virus-infected cells (Fig. 6C). These results suggest that these mutations did not affect the replication of the viral genome or the translation of viral proteins. To verify whether the transport of vRNP is impaired in cells infected with these mutant viruses, the localization of vRNP and co-localization of vRNP and Rab11 were analyzed. MDCK cells expressing FLAG-Rab11 (MDCK-F11A-WT) were infected with each mutant virus, and cells were stained for vRNP and FLAG-Rab11 10 hpi using an anti-NP monoclonal antibody that preferentially binds to NP in the RNP form and the anti-FLAG polyclonal antibody. The results indicate that localization of vRNP and co-localization of vRNP and FLAG-Rab11 were not affected by these mutations (Fig. 6D).

To investigate the effects of the mutations on viral genome packaging and budding of progeny virion, HA and plaque titers of the mutant viruses were determined. HA titer correlates with particle counts and plaque titer reflects the infectious particle counts. MDCK cells were infected with each mutant virus at an MOI of 1, and the HA and plaque assays were performed using the supernatant at 24 hpi. HA titers of mutant viruses were comparable to that of the M2stop virus, whereas plaque titers of mutant viruses were reduced compared to that of the M2stop virus (Fig. 7A). To confirm the result of the HA assay, the number of virus particles in the supernatant was counted under electron microscopy. The number of mutant virus particles was comparable to that of M2stop virus particles (Fig. 7A). These results suggest that the ratios of infectious particle to total virus particle was reduced in the supernatant from cells infected with the mutant viruses. Next, we analyzed the amount of viral proteins and vRNAs in the supernatant from cells infected with each mutant virus. MDCK cells were infected with each mutant virus at an MOI of 1, and the supernatants were collected at 24 hpi. The virus particles were concentrated by ultracentrifugation of the supernatant. The amounts of HA, NP, and M1 in the supernatants from cells infected with each mutant virus were comparable to those from the cells infected with the M2stop virus (Fig. 7B and C). In contrast, the amounts of vRNA segments in the supernatants from cells infected with each mutant virus were approximately 40% lower than those from the M2stop virus-infected cells (Fig. 7D). These results suggest that the viral genome packaging efficiency specifically decreased in the cells infected with these mutant viruses. We next determined the amounts of viral proteins associated with the lipid raft fraction of cells infected with each mutant virus because progeny virion budding occurs at membrane lipid rafts (Scheiffele et al., 1997; Chen et al., 2005, 2007; Leser and Lamb, 2005). The amounts of viral proteins in the lipid raft fractions from cells infected with each mutant virus were also comparable to those from the cells infected with the M2stop virus (Fig. S1).

Next, we analyzed whether all segments were bundled and co-packaged in these mutant viruses. If the number of virions that

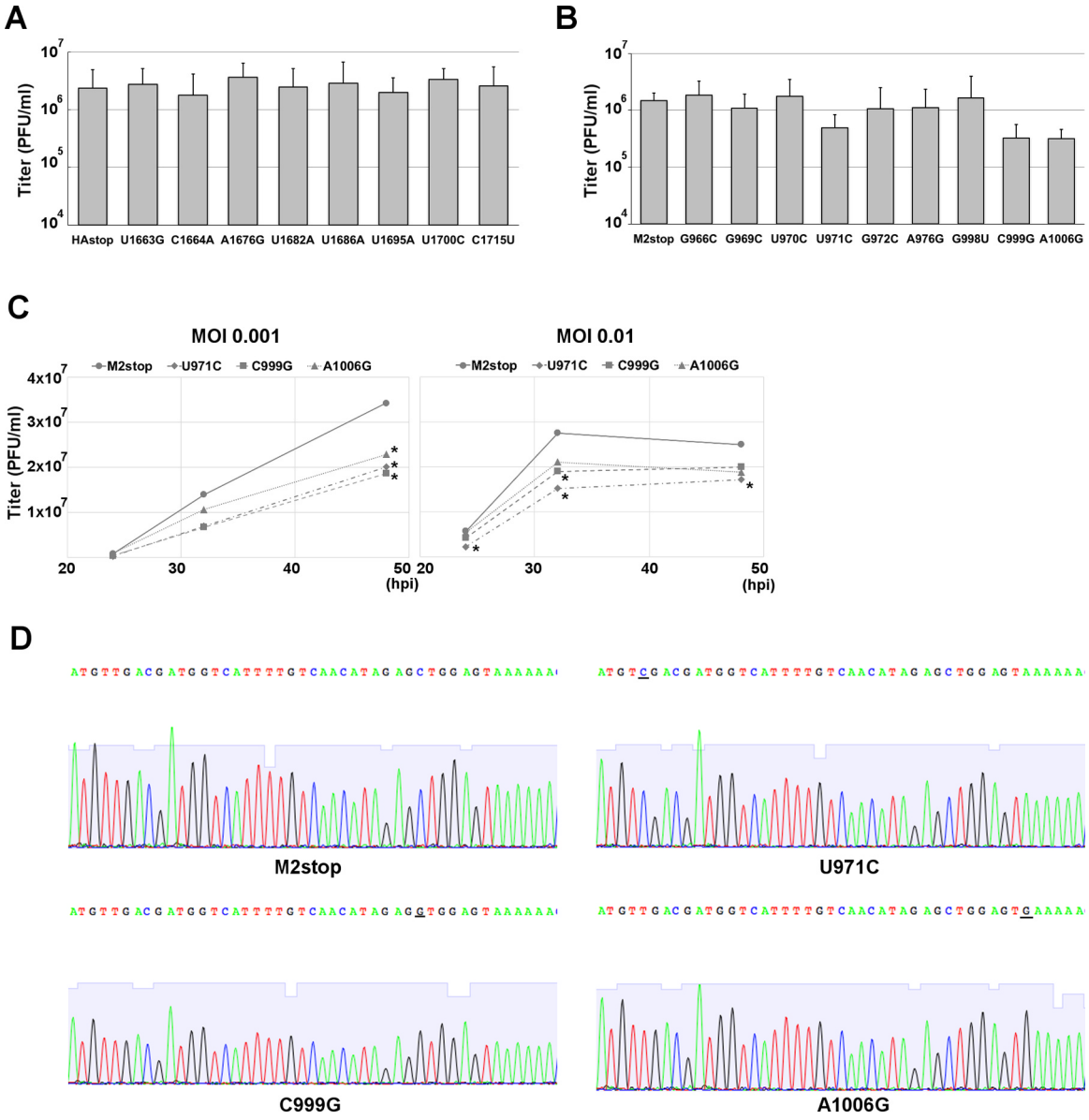

Fig. 5. Propagation of recombinant viruses containing a single mutation in the selected nucleotide residues. The titer of recombinant viruses containing a single mutation in segment 4 (A) or segment 7 (B). MDCK-HA or MDCK-M2 cells were infected with the recombinant virus containing a single mutation in segment 4 at an MOI of 0.01 (A) or that in segment 7 at an MOI of 0.001 (B), respectively. The cells were incubated with trypsin, and the supernatant was collected at 24 hpi. The viral titers in the supernatants were determined by plaque assay. The graph indicates average values with standard deviations from three independent experiments. (C) The growth curve of the M2stop virus and the M2stop virus containing the U971C, C999G, or A1006G mutation. MDCK-M2 cells were infected with each recombinant virus containing a single mutation at an indicated MOI. The cells were incubated with trypsin, and the supernatant was collected at 24, 32, and 48 hpi. The viral titers were determined by plaque assay. The graph presents average values from five independent experiments. *P*-values were calculated by the Student's *t*-test and the Benjamini-Hochberg multiple-test correction method. $*P < 0.05$. (D) Segment 7 sequence of M2stop and mutant viruses. MDCK-M2 cells were infected with each mutant virus at an MOI of 0.001, and the supernatant was collected at 48 hpi. The viral RNA in the supernatant was purified and the sequence was determined after RT-PCR.

successfully packaged all eight segments decreased, the fraction of semi-infectious (SI) particles relative to all infectious virions should increase. These SI virions might fail to express some viral proteins because of the absence of segments encoding the viral proteins, as shown in previous studies (Brooke et al., 2014). We therefore performed an immunostaining analysis of viral proteins in the cells infected with these mutant viruses to estimate the fraction of SI particles. Single- and double-stained cells were counted, and the ratios of the number of double-stained cells to the number of single- and double-stained cells were calculated. In either combination, the ratios of double-positive cells were comparable to that of the cells infected with M2stop virus (Fig. S2). These results suggest that all eight segments were probably bundled and co-packaged in these single point mutation viruses.

3.4. Impairment of viral genome packaging by single mutations at positions U971 and A1006 in segment 7 of wild type virus

We identified the three nucleotide residues in segment 7 involved in efficient viral genome packaging using M2stop virus and MDCK-M2 cells. One mutation, C999G, is nonsynonymous while other two mutations, U971C and A1006G, are synonymous. Thus, to confirm the impairment of viral genome packaging by a single mutation at the identified nucleotide residues, viral genome packaging of mutant virus containing U971C or A1006G mutation not in M2stop virus but in wild

type virus was analyzed. First, the amounts of viral proteins and vRNA in infected cells were determined. The amounts of HA, NP, and M1 in the cells infected with the virus containing the U971C or A1006G mutation at 8 hpi were comparable to those in cells infected with the

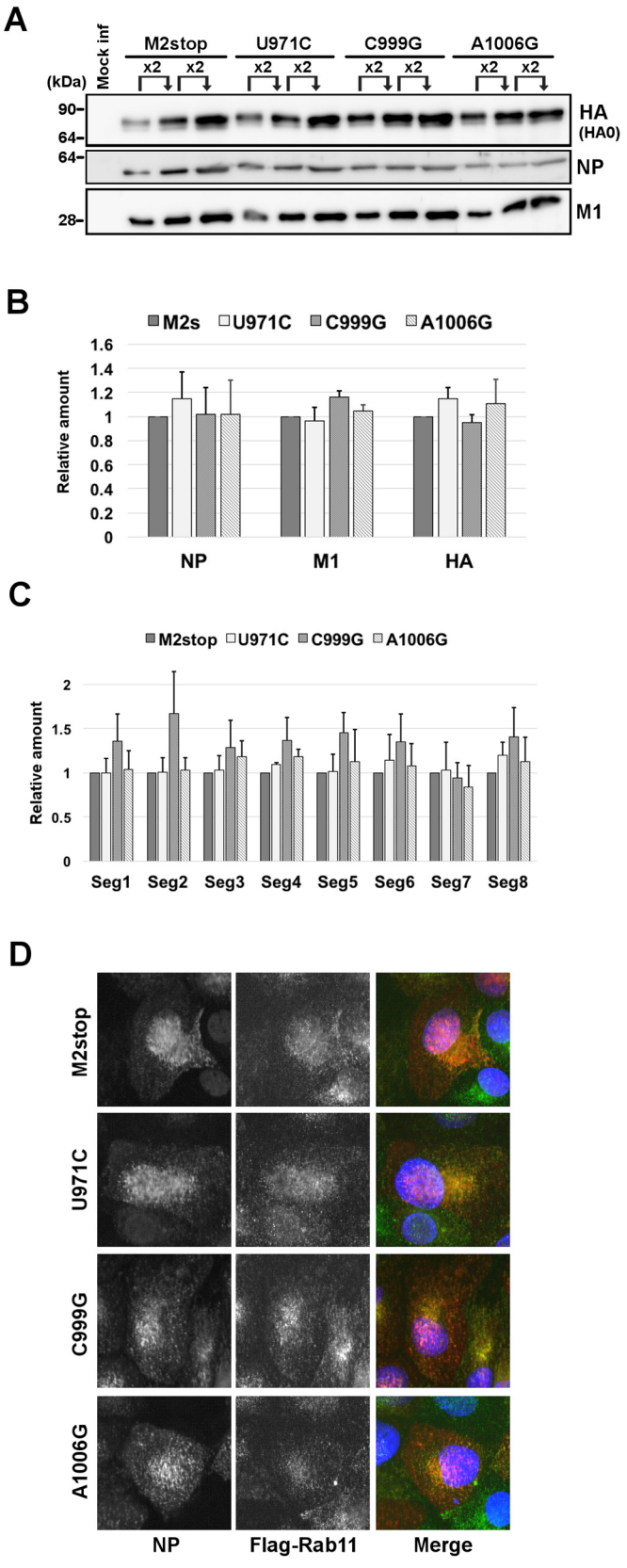

Fig. 6. Amounts of viral proteins and vRNAs in cells infected with M2stop virus containing the U971C, C999G, and A1006G mutations. (A) The detection of viral proteins in infected cells. MDCK cells were infected with M2stop virus or M2stop virus containing the U971C, C999G, or A1006G mutation at an MOI of 1. The cells were collected at 8 hpi, and HA, NP, and M1 were detected by western blotting. The ratio of the loaded sample volumes was 1:2:4. (B) The relative amounts of HA, NP, and M1 in cells infected with the mutant viruses. The band intensities in (A) were measured and standard curves were obtained. The amount of each viral proteins in cells infected with mutant virus relative to that with M2stop virus was semi-quantified from the standard curves. The graph indicates average values with standard deviations from three independent experiments. (C) The relative amount of vRNAs in cells infected with the mutant viruses. Total RNA was extracted with the same samples used in (A) and the amount of each vRNA segment in cells infected with mutant virus relative to that with M2stop virus was determined by RT-qPCR. The graph indicates average values with standard deviations from three independent experiments. (D) Co-localization of NP and Flag-Rab11 in cells infected with the mutant viruses. MDCK-F11-WT cells were infected with the mutant viruses and the parent M2stop virus at an MOI of 3. At 10 hpi, vRNP (NP) and FLAG-Rab11 were visualized by indirect immunofluorescence assay. Specimens were observed under a confocal microscope. Red: NP, Green: FLAG-Rab11, Blue: Hoechst33343.

wild type virus (Fig. 8A). The amounts of vRNA segments in the U971C mutant virus-infected cells were comparable to those in the wild type virus-infected cells (Fig. 8B). The amount of segment 7 vRNA in the A1006G mutant virus-infected cells were slightly reduced compared to that in the wild type virus-infected cells (Fig. 8B). These results suggest that U971C or A1006G mutation in segment 7 of wild type virus did not affect the translation of viral proteins and slightly affected the synthesis of viral RNA. Next, HA and plaque titers of the mutant viruses were determined. MDCK cells were infected with each mutant virus at an MOI of 1, and HA assay and plaque assays were performed using the supernatant at 24 hpi. HA titers of U971C and A1006G mutant viruses were comparable to that of the wild type virus, whereas plaque titers of the mutant viruses were reduced (Fig. 9A). Next, we analyzed the amount of viral proteins and vRNAs in the supernatant from cells infected with the mutant viruses. MDCK cells were infected with each mutant virus at an MOI of 1, and the supernatants were collected at 24 hpi. The virus particles were concentrated by ultracentrifugation of the supernatant. The amounts of HA, NP, and M1 in the supernatants from cells infected with U971C and A1006G mutant viruses were comparable to those from the cells infected with the wild type virus (Fig. 9B). *P*-values of each segment amount changes were calculated by the Student's *t*-test and the Benjamini-Hochberg multiple-test correction method and those of total vRNA amount changes were calculated by the Tukey-Kramer method. The amounts of vRNA segments in the supernatants from cells infected with the mutant viruses were slightly reduced compared to those from the wild type virus-infected cells (Fig. 9C; the adjusted *P*-values of the total vRNA amount changes between wild type and U971C virus and between wild type and A1006G virus were 2.5×10^{-6} and 1.8×10^{-4}, respectively). Taken together, these results suggest that the viral genome packaging efficiency decreased even in cells infected with the recombinant virus containing the U971C or A1006G mutation in segment 7 of the wild type virus.

3.5. Alteration of local vRNP structure by the introduction of a single mutation at position C999 or A1006 in segment 7

We revealed that a single mutation at each of the three identified nucleotide residues affects the packaging efficiency of bundled vRNPs. However, the mechanism by which these single mutations reduce the packaging efficiency is still unclear. Nucleotide positions between 967 and 994 in segment 7, which are predicted to form a stem-loop structure, are conserved in wild-type strains, and a mutant virus containing mutations that disrupt the predicted stem-loop structure had attenuated infectivity (Spronken et al., 2017; Kobayashi et al., 2016). Thus, we

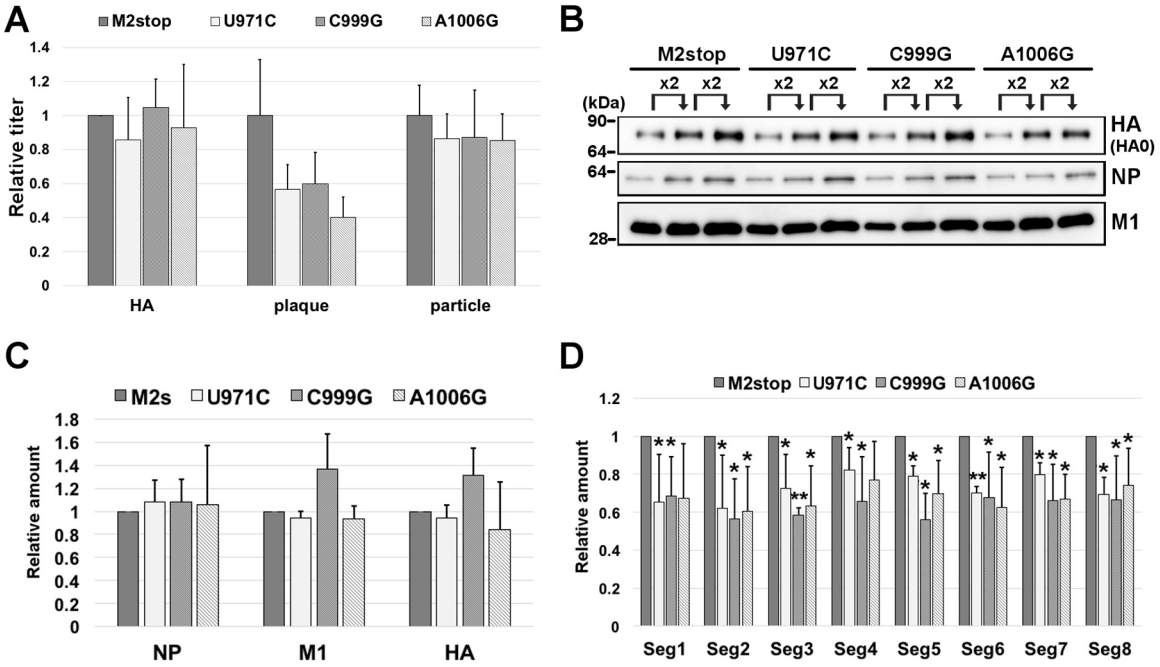

Fig. 7. Effect of U971C, C999G, and A1006G mutations in M2stop virus on segment packaging. (A) HA, plaque, and particle titer of mutant viruses. MDCK cells were infected with M2stop virus or M2stop virus containing the U971C, C999G, or A1006G mutation at an MOI of 1. The cells were incubated without trypsin, and the supernatant was collected at 24 hpi. HA titer and plaque titer of the supernatant from cells infected with mutant virus relative to that with M2stop virus were determined by HA assay and plaque assay, respectively. The graph indicates average values with standard deviations from three independent experiments. MDCK cells were infected with the M2stop or mutant virus at an MOI of 0.01. The supernatant was collected at 48 hpi and virus particles were pelleted through a sucrose cushion. Particle titer was determined by electron microscopy observation. The graph indicates relative values with standard deviations from 10 independent views representing a total of 1800–2100 particles. (B) The detection of viral proteins in mutant viruses. MDCK cells were infected with M2stop virus or M2stop virus containing the U971C, C999G, or A1006G mutation at an MOI of 1. The supernatant was collected at 24 hpi, and virus in the supernatant was concentrated by ultracentrifugation. HA, NP, and M1 were detected by western blotting. The ratio of the loaded sample volumes was 1:2:4. (C) Relative amounts of HA, NP, and M1 in mutant viruses. The band intensities in (B) were measured and standard curves were generated. The amount of each viral protein in mutant virus relative to that in the M2stop virus was semi-quantified from the standard curves. The graph indicates average values with standard deviations from three independent experiments. (D) The relative amount of vRNAs in mutant viruses. The vRNA was extracted with the same samples used in (B) and the amount of each vRNA segment in mutant virus relative to that with M2stop virus was determined by RT-qPCR. The graph indicates average values with standard deviations from three independent experiments. P-values were calculated by the Student's *t*-test and the Benjamini-Hochberg multiple-test correction method. $**P < 0.01$ and $*P < 0.05$.

hypothesized that introducing single mutations at positions U971, C999, and A1006 induces local vRNP structural changes. To test this hypothesis, vRNPs in the virions were chemically modified by treatment with DMS or NAI. DMS methylates accessible N1 of adenosine and N3 of cytidine, and NAI modifies each 2′-OH group in the ribose backbone in single-stranded RNA. The modified nucleotides can be detected by primer extension assay because reverse transcription by M-MLV reverse transcriptase is blocked at the modified sites. Using this method, the accessibility of the mutation site to DMS and NAI was determined. The mutant viruses and parent M2stop viruses were treated with DMS or NAI, and a primer extension assay was performed. In the A1006G mutant virus, a band corresponding to A1003 disappeared when the mutant virus was treated with NAI (Fig. 10A). In the C999G mutant virus, a band corresponding to A997 appeared when treated with DMS (Fig. 10A). No significant differences in modified nucleotides were observed between the parental M2stop virus and U971C mutant virus. To confirm that these two single mutations (A1006G and C999G) altered the accessibility of these RNA modification reagents to vRNA only in the vRNP form, the accessibility of DMS and NAI to the *in vitro* synthesized segment 7 vRNA that contained each of the two mutations was determined. In both mutants, the nucleotides modified by DMS and NAI were different between vRNP and vRNA and the mutation specific RNA modification observed in the vRNP templates did not occur in the vRNA templates (Fig. 10B). These results suggest that the local vRNP structure in the virion is altered by introducing a single point mutation at positions C999 and A1006, at least.

4. Discussion

Previous studies identified several specific residues in segments 4 and 7 that are involved in genome packaging by introducing mutations in the BSs (Hutchinson et al., 2008; Marsh et al., 2007). In the experimental conditions employed in these studies, however, only synonymous mutations could be introduced in the BSs. To overcome this limitation, we constructed recombinant virus libraries, in which each virus contained a random sequence in the BSs of segments 4 and 7 and screened for mutant viruses that could propagate in cells expressing the viral proteins (HA or M2). Using this method, we showed that the viruses containing various sequences randomly introduced in the BS of segments 4 and 7 remained after 5 passages (Fig. 2) and identified several residues that might be required for efficient genome packaging (Figs. 4 and 5). A previous report showed that positions 979–1007 of segment 7 can be replaced by highly diverse sequences without significant effects on the virus propagation (Ozawa et al., 2009). We show that positions 1656–1666 and 1676–1727 of segment 4 and positions 960–1005 of segment 7 can vary without impairing the efficiency of virus propagation (Fig. 2). In addition, we identified nucleotide residues required for efficient genome packaging without considering the effects of amino acid sequence changes (Figs. 4 and 5). Previous studies also identified conserved residues required for efficient genome packaging and bundling (Zhao et al., 2014; Hutchinson et al., 2008, 2009; Marsh et al., 2007, 2008). These results indicate that nucleotide residues both involved in and not involved in efficient genome packaging and bundling exist in BSs.

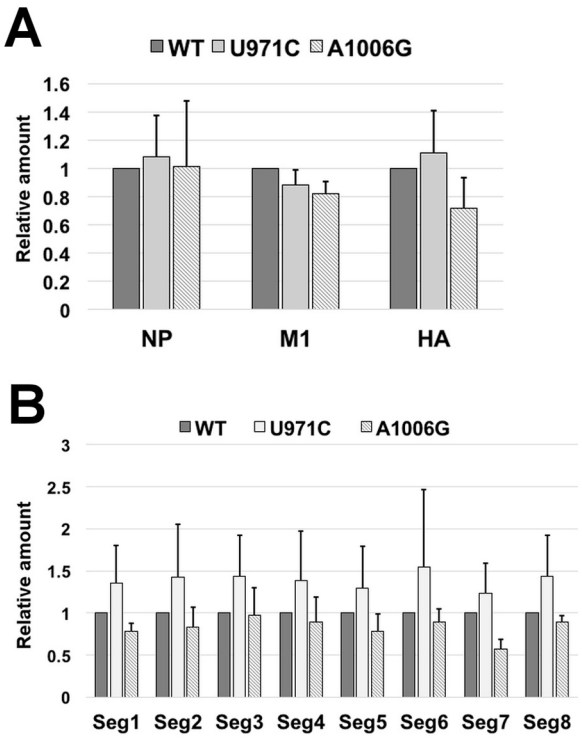

Fig. 8. The amount of viral proteins and vRNAs in cells infected with recombinant virus containing the U971C and A1006G mutations in wild type virus. (A) The relative amounts of HA, NP, and M1 in mutant virus infected cells. MDCK cells were infected with wild type or mutant virus containing the U971C or A1006G mutation at an MOI of 1. The cells were collected at 8 hpi, and HA, NP, and M1 were detected by western blotting. The band intensities were measured, and standard curves were generated. The amount of each viral protein in cells infected with mutant virus relative to that with wild type virus was semi-quantified from the standard curves. The graph indicates average values with standard deviations from three independent experiments. WT: wild type virus. (B) The relative amount of vRNAs in cells infected with the mutant viruses. Total RNA was extracted from the same samples used in (A) and the amount of each vRNA segment in cells infected with mutant virus relative to that with wild type virus was determined by RT-qPCR. The graph indicates average values with standard deviations from three independent experiments.

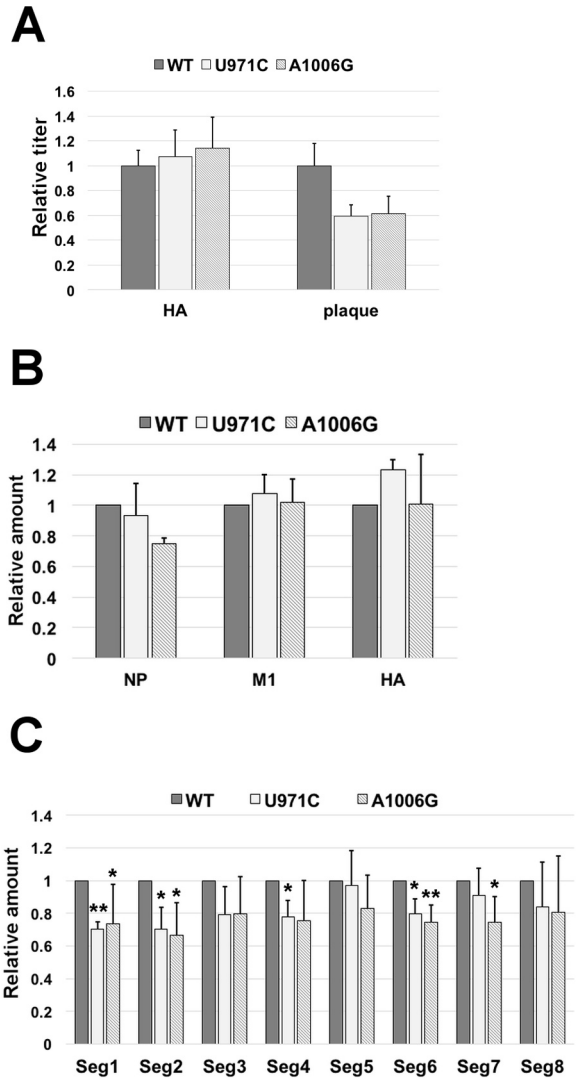

Fig. 9. Effect of U971C and A1006G mutations in wild type virus on segment packaging. (A) HA and plaque titer of mutant viruses. MDCK cells were infected with wild type or mutant virus containing the U971C or A1006G mutation at an MOI of 1. The cells were incubated without trypsin, and the supernatant was collected at 24 hpi. HA titer and plaque titer of the supernatant from cells infected with mutant virus relative to that with wild type virus were determined by HA assay and plaque assay, respectively. The graph indicates average values with standard deviations from three independent experiments. (B) The relative amounts of HA, NP, and M1 in mutant viruses. MDCK cells were infected with wild type or mutant virus containing the U971C or A1006G mutation at an MOI of 1. The supernatant was collected at 24 hpi, and virus in the supernatant was concentrated by ultracentrifugation. HA, NP, and M1 were detected by western blotting. The band intensities were measured, and standard curves were generated. The amount of each viral proteins in mutant virus relative to that in wild type virus was semi-quantified from the standard curves. The graph indicates average values with standard deviations from three independent experiments. (C) The relative amount of vRNAs in mutant viruses. The vRNA was extracted from the same samples used in (B) and the amount of each vRNA segment in mutant virus relative to that with wild type virus was determined by RT-qPCR. The graph indicates average values with standard deviations from three independent experiments. *P*-values were calculated by the Student's *t*-test and the Benjamini-Hochberg multiple-test correction method. $^{*}P < 0.05$.

Among the segment 7 mutants that contained single mutations at selected residues, three mutants (U971C, C999G, and A1006G) showed a defect in genome packaging but not in genome bundling (Figs. 4–7, and S2). However, in our analysis, segment 4 mutant viruses that contain single mutations at selected residues did not show a significant reduction in virus propagation, and the three viruses with mutations in segment 7 did not show a defect in genome bundling (Figs. 4–7, and S2), indicating that these single mutations in the BSs had little effect on segment bundling. The single mutation could only induce local structure changes of vRNP and had little effect on RNA-RNA interaction between segments. A segment bundling defect was previously observed in a recombinant virus containing multiple synonymous mutations in segment 4 and segment 7 (Hutchinson et al., 2008; Marsh et al., 2007). Marsh et al. showed that segment bundling was impaired in recombinant virus containing 9 synonymous mutations in nucleotide positions 1659 – 1673 of segment 4 and Hutchinson et al. showed that segment bundling was impaired in recombinant viruses containing 3 synonymous mutations in nucleotide positions 983 – 989 of segment 7. In addition, viruses containing one or two nucleotide deletions in the random sequence-introduced region were enriched after 5 passages (Fig. 2). These deletions would not induce vRNP structural changes, and thus, the viruses can propagate efficiently. The multiple mutations and large deletions in the BSs could induce global structure changes and/or affect multiple RNA-RNA interactions between segments, and thus, these multiple mutations or deletion of BS would induce not only genome packaging but also segment bundling defects. While viral genome packaging of mutant viruses was impaired, the amount of NP in the virion was not reduced, except for a mutant virus containing

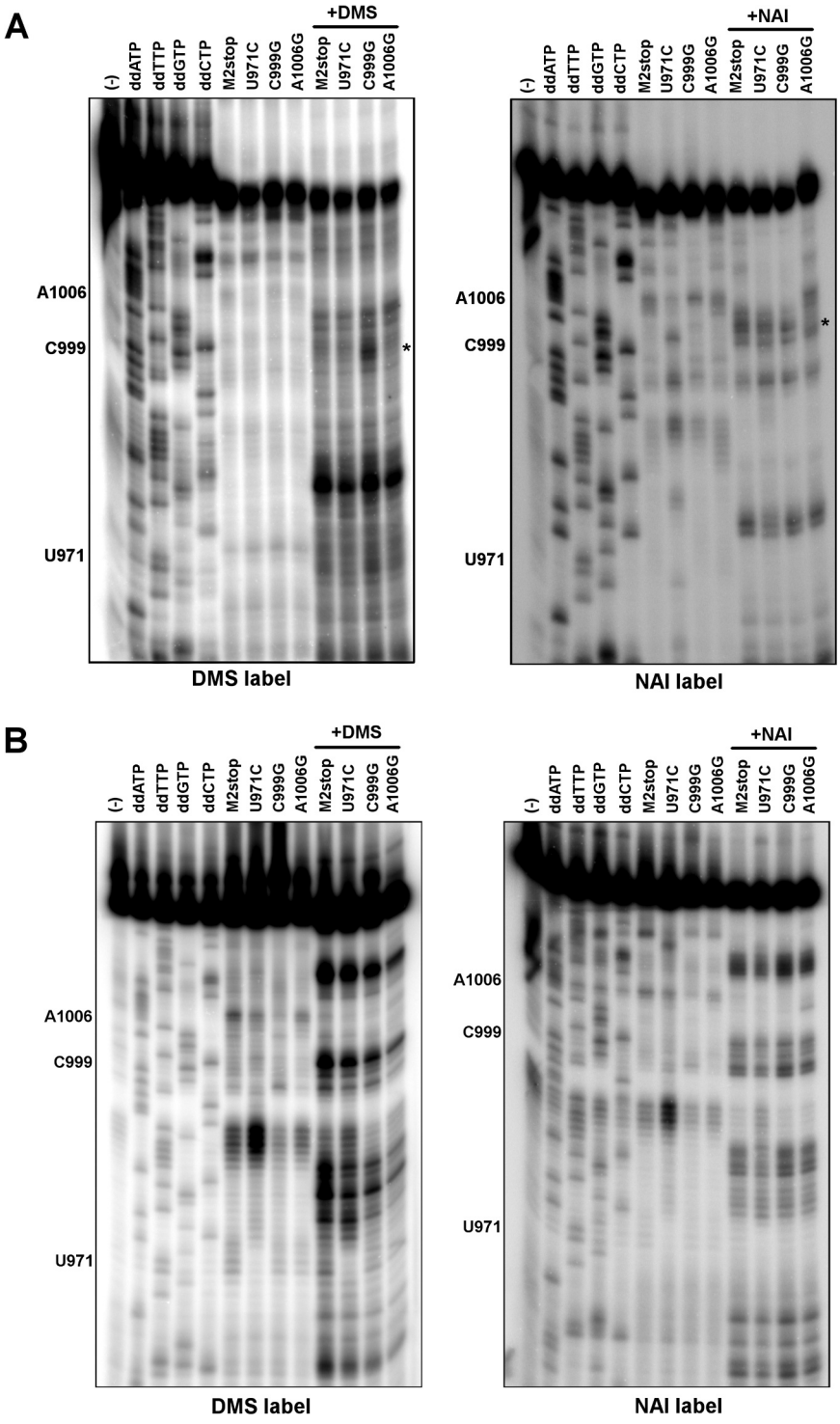

Fig. 10. Accessibility of the vRNP to RNA modification reagents in the mutant viruses. (A) DMS and NAI treatment of the mutant viruses. The mutant viruses and the parent M2stop virus were treated with DMS or NAI, and a primer extension assay was performed. The nucleotide sequences were determined using *in vitro* synthesized segment 7 RNA and ddNTPs. *: key nucleotides modified with DMS or NAI. (B) DMS and NAI treatment of the synthesized segment 7 vRNAs. The T7 synthesized segment 7 vRNAs each containing a single mutation were treated with DMS or NAI for 3 or 10 min, respectively, and a primer extension assay was performed.

A1006G mutations in the wild type virus (Figs. 7C and 9B). A previous study suggests that host-derived 18S and 28S rRNAs were incorporated in the virion (Noda et al., 2018), and thus, rRNAs may be incorporated in the mutant viruses with NP but not in the A1006G mutant virus for an unknown reason.

Propagation of mutant viruses containing the U971C or A1006G mutation in the wild type virus was reduced compared with that of the wild type virus (Fig. 9A). However, the packaging defect of mutant viruses containing mutation in wild type virus was less pronounced than that in the M2stop virus (Figs. 7D and 9C). Premature termination codons inserted for generating the M2stop virus were located in BS of segment 7. Inserted premature termination codons do not affect viral genome packaging and segment bundling, but the U971C or A1006G mutation and the inserted premature termination codons may exert a synergistic effect to alter vRNP structures.

The accessibility of DMS and NAI was different between vRNAs and vRNPs (Fig. 10). The vRNA is complexed with the viral RNA polymerase complexes and NP in infected cells and virions. Although a previous report suggested that a functional stem-loop structure can be formed in the vRNP structure (York et al., 2013), the vRNA-protein interactions, especially those between vRNA and NP, might disrupt some secondary structures of vRNA and prevent the access of these RNA modification

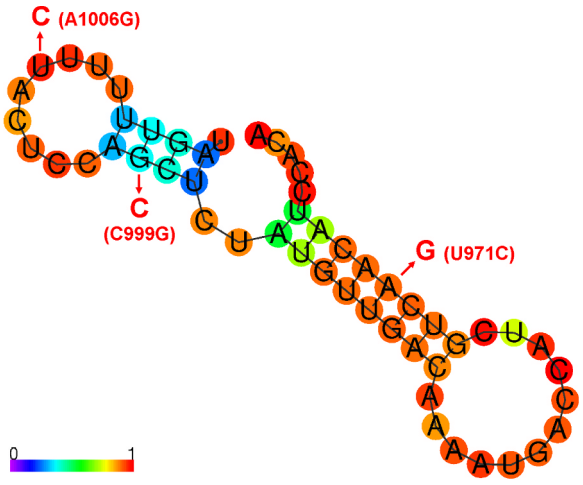

Fig. 11. Predicted secondary structure at nucleotide positions 14–66 of segment 7 vRNA. the secondary structure was predicted at nucleotide positions 14–66 of segment 7 vRNA (corresponding to nucleotide positions 962–1014 in the positive-sense orientation). The red arrows and nucleotides indicate the positions and mutations corresponding to U971C, C999G, and A1006G. The background color of each base represents the base pairing probabilities.

reagents to the target nucleotides. A computational analysis of the conserved vRNA secondary structures in segment 7 predicted a stem-loop structure at nucleotide positions 967 – 994 of segment 7 vRNA, and the titer of a recombinant virus that contained mutations disrupting the predicted stem-loop structure was slightly reduced compared to that of the wild-type virus (Spronken et al., 2017; Kobayashi et al., 2016), suggesting the involvement of this stem-loop structure in viral propagation. In addition, nucleotide positions around 967 – 994 were a low NP coverage region in the WSN strain (Lee et al., 2017). The secondary structure at nucleotide positions 962 – 1014 of segment 7 vRNA predicted by CentroidFold is shown in Fig. 11 (Hamada et al., 2009). The accessibility of DMS and NAI to nucleotide positions between A967 and A993 is consistent with the predicted stem-loop structure of this region, indicating that this region could form a stem-loop structure in the virion (Fig. 10). The accessibility of DMS and NAI to the vRNP in the U971C mutant virion was comparable to that in the M2stop virion (Fig. 10A). However, U971 is located in the middle of a long stem in the predicted secondary structure (Fig. 11) and is conserved among wild-type virus strains in the database, even though it is located in the third codon position. A computational analysis suggested that the U971C mutation did not disrupt the stem-loop structure, but the base pairing probability value of the stem structure was reduced by the mutation. Thus, the U971C mutation may destabilize the stem-loop structure and impair genome packaging. Another possibility is that the destabilization of the stem-loop structure by the U971C mutation indirectly induces vRNP structural changes that were not detectable in our analysis. In contrast, the accessibility of DMS and NAI to the vRNPs of the C999G and A1006G mutants clearly changed around the mutation sites (Fig. 10A). This indicates that these mutations induced some structural changes in this region. In addition, the different accessibilities of DMS and NAI around C999 and A1006 between vRNPs in the virion and *in vitro* synthesized vRNA (Fig. 10) indicate that the vRNA-NP interaction alters the secondary structure of vRNA. Generally, stem-loop structures play important roles in intermolecular RNA-RNA interactions by forming a kissing loop structure (Paillart et al., 1996). These mutations would induce the dissociation of cis- or trans-segment RNA interaction, resulting in inefficient genome packaging. Further investigations are required to reveal whether these nucleotide residues are involved in intermolecular RNA interactions.

Another notable finding is that the wild-type sequence was highly enriched in the segment 4 1676N library after passaging (Fig. 2). However, the percentage of wild-type sequence in the plasmid library that was used to construct the 1676N virus library was exceptionally high at approximately 4.6% in this library compared to 0.002–0.52% in other libraries (Table S3 and S1 File). Thus, the wild-type sequence-containing virus was already overrepresented in this library even before the selection. Since the wild-type sequence should be one of the most preferable sequences for virus propagation, the wild-type sequence-containing virus was probably further enriched by passaging.

In conclusion, we identified three nucleotide residues required for efficient genome packaging in the BS of segment 7 and revealed that point mutations at these nucleotide positions induce local structural changes. An interesting and somewhat unexpected effect of these mutations was that they impaired only genome packaging but not segment bundling. Although additional studies are required to reveal the actual secondary and higher order structures of vRNP and their roles in genome packaging and bundling, the findings will help us to better understand the role(s) of BSs in genome packaging and bundling in influenza virus and further highlight the roles of secondary and higher order structures of vRNP in these processes. Our findings may have significant impacts on studies of other RNA viruses and those with segmented genomes.

Acknowledgements

We thank Dr. Yoshihiro Kawaoka (University of Tokyo) for kindly providing plasmids for reverse genetics system, Dr. Kyosuke Nagata (University of Tsukuba) for kindly providing anti-NP antibody, and Dr. Nobuyuki Kobayashi (Nagasaki University) for kindly providing anti-M1 antibody. We thank Dr. Takaho A. Endo (RIKEN) for helpful discussions, and Ms. Yukiko Iwata for technical support of experiments.

Funding

This work was supported by JSPS KAKENHI [JP25871077 and JP15K21607 to N.T.]; and MEXT KAKENHI [JP221S0002 to N.T., Y.O., T.H., and K.K.]. This research was partially supported by Platform Project for Supporting Drug Discovery and Life Science Research (Basis for Supporting Innovative Drug Discovery and Life Science Research (BINDS)) from AMED under Grant Number JP18am0101070.

Appendix A. Supplementary material

Supplementary data associated with this article can be found in the online version at doi:10.1016/j.virol.2019.03.004.

References

Amorim, M.J., Bruce, E.A., Read, E.K.C., Foeglein, A., Mahen, R., Stuart, A.D., Digard, P., 2011. A Rab11- and microtubule-dependent mechanism for cytoplasmic transport of influenza A virus viral RNA. J. Virol. 85, 4143–4156.

Brooke, C.B., Ince, W.L., Wei, J., Bennink, J.R., Yewdell, J.W., 2014. Influenza A virus nucleoprotein selectively decreases neuraminidase gene-segment packaging while enhancing viral fitness and transmissibility. Proc. Natl. Acad. Sci. USA 111, 16854–16859.

Chen, B.J., Takeda, M., Lamb, R.A., 2005. Influenza virus hemagglutinin (H3 subtype) requires palmitoylation of its cytoplasmic tail for assembly: M1 proteins of two subtypes differ in their ability to support assembly. J. Virol. 79, 13673–13684.

Chen, B.J., Leser, G.P., Morita, E., Lamb, R.A., 2007. Influenza virus hemagglutinin and neuraminidase, but not the matrix protein, are required for assembly and budding of plasmid-derived virus-like particles. J. Virol. 81, 7111–7123.

Chou, Y.Y., Vafabakhsh, R., Doganay, S., Gao, Q., Ha, T., Palese, P., 2012. One influenza virus particle packages eight unique viral RNAs as shown by FISH analysis. Proc. Natl. Acad. Sci. 109, 9101–9106.

Chou, Y.Y., Heaton, N.S., Gao, Q., Palese, P., Singer, R., Lionnet, T., 2013. Colocalization of different influenza viral RNA segments in the cytoplasm before viral budding as shown by single-molecule sensitivity FISH analysis. PLoS Pathog. 9, e1003358. https://doi.org/10.1371/journal.ppat.1003358.

Eisfeld, A.J., Kawakami, E., Watanabe, T., Neumann, G., Kawaoka, Y., 2011. RAB11A is essential for transport of the influenza virus genome to the plasma membrane. J. Virol. 85, 6117–6126.

Fournier, E., Moules, V., Essere, B., Paillart, J.-C., Sirbat, J.-D., Isel, C., Cavalier, A., Rolland, J.-P., Thomas, D., Lina, B., Marquet, R., 2012. A supramolecular assembly formed by influenza A virus genomic RNA segments. Nucleic Acids Res 40, 2197–2209.

Gavazzi, C., Yver, M., Isel, C., Smyth, R.P., Rosa-Calatrava, M., Lina, B., Moulès, V., Marquet, R., 2013a. A functional sequence-specific interaction between influenza A virus genomic RNA segments. Proc. Natl. Acad. Sci. USA 110, 16604–16609.

Gavazzi, C., Isel, C., Fournier, E., Moules, V., Cavalier, A., Thomas, D., Lina, B., Marquet, R., 2013b. An in vitro network of intermolecular interactions between viral RNA segments of an avian H5N2 influenza A virus: comparison with a human H3N2 virus. Nucleic Acids Res 41, 1241–1254.

Gerber, M., Isel, C., Moules, V., Marquet, R., 2014. Selective packaging of the influenza A genome and consequences for genetic reassortment. Trends Microbiol 22, 446–455.

Giese, S., Bolte, H., Schwemmle, M., 2016. The Feat of Packaging Eight Unique Genome Segments. Viruses 8, 165.

Gilbertson, B., Zheng, T., Gerber, M., Printz-Schweigert, A., Ong, C., Marquet, R., Isel, C., Rockman, S., Brown, L., 2016. Influenza NA and PB1 Gene Segments Interact during the Formation of Viral Progeny: localization of the Binding Region within the PB1 Gene. Viruses 8, 238.

Gog, J.R., Afonso, E.D.S., Dalton, R.M., Leclercq, I., Tiley, L., Elton, D., von Kirchbach, J.C., Naffakh, N., Escriou, N., Digard, P., 2007. Codon conservation in the influenza A virus genome defines RNA packaging signals. Nucleic Acids Res 35, 1897–1907.

Goto, H., Muramoto, Y., Noda, T., Kawaoka, Y., 2013. The genome-packaging signal of the influenza A virus genome comprises a genome incorporation signal and a genome-bundling signal. J. Virol. 87, 11316–11322.

Hamada, M., Kiryu, H., Sato, K., Mituyama, T., Asai, K., 2009. Prediction of RNA secondary structure using generalized centroid estimators. Bioinformatics 25, 465–473.

Hutchinson, E., Fodor, E., 2013. Transport of the influenza virus genome from nucleus to nucleus. Viruses 5, 2424–2446.

Hutchinson, E.C., Curran, M.D., Read, E.K., Gog, J.R., Digard, P., 2008. Mutational analysis of cis-acting RNA signals in segment 7 of influenza A virus. J. Virol. 82, 11869–11879.

Hutchinson, E.C., Wise, H.M., Kudryavtseva, K., Curran, M.D., Digard, P., 2009. Characterisation of influenza A viruses with mutations in segment 5 packaging signals. Vaccine 27, 6270–6275.

Kawaguchi, A., Momose, F., Nagata, K., 2011. Replication-coupled and host factor-mediated encapsidation of the influenza virus genome by viral nucleoprotein. J. Virol. 85, 6197–6204.

Kobayashi, Y., Dadonaite, B., Doremalen, N. Van, Barclay, W.S., Pybus, O.G., 2016. Computational and molecular analysis of conserved influenza A virus RNA secondary structures involved in infectious virion production. RNA Biol. 13, 883–894.

Lakdawala, S.S., Wu, Y., Wawrzusin, P., Kabat, J., Broadbent, A.J., Lamirande, E.W., Fodor, E., Altan-Bonnet, N., Shroff, H., Subbarao, K., 2014. Influenza A virus assembly intermediates fuse in the cytoplasm. PLoS Pathog. 10, e1003971. https://doi.org/10.1371/journal.ppat.1003971.

Lee, N., Le Sage, V., Nanni, A.V., Snyder, D.J., Cooper, V.S., Lakdawala, S.S., 2017. Genome-wide analysis of influenza viral RNA and nucleoprotein association. Nucleic Acids Res 45, 8968–8977.

Leser, G.P., Lamb, R.A., 2005. Influenza virus assembly and budding in raft-derived microdomains: a quantitative analysis of the surface distribution of HA, NA and M2 proteins. Virology 342, 215–227.

Marsh, G.A., Hatami, R., Palese, P., 2007. Specific residues of the influenza A virus hemagglutinin viral RNA are important for efficient packaging into budding virions. J. Virol. 81, 9727–9736.

Marsh, G.A., Rabadan, R., Levine, A.J., Palese, P., Rabadán, R., Levine, A.J., Palese, P., 2008. Highly conserved regions of influenza A Virus polymerase gene segments are critical for efficient viral RNA packaging. J. Virol. 82, 2295–2304.

Momose, F., Kikuchi, Y., Komase, K., Morikawa, Y., 2007. Visualization of microtubule-mediated transport of influenza viral progeny ribonucleoprotein. Microbes Infect. 9, 1422–1433.

Momose, F., Sekimoto, T., Ohkura, T., Jo, S., Kawaguchi, A., Nagata, K., Morikawa, Y., 2011. Apical transport of influenza A virus ribonucleoprotein requires Rab11-positive recycling endosome. PLoS One 6, e21123. https://doi.org/10.1371/journal.pone.0021123.

Muramoto, Y., Takada, A., Fujii, K., Noda, T., Iwatsuki-Horimoto, K., Watanabe, S., Horimoto, T., Kida, H., Kawaoka, Y., 2006. Hierarchy among viral RNA (vRNA) segments in their role in vRNA incorporation into influenza A virions. J. Virol. 80, 2318–2325.

Neumann, G., Watanabe, T., Ito, H., Watanabe, S., Goto, H., Gao, P., Hughes, M., Perez, D.R., Donis, R., Hoffmann, E., Hobom, G., Kawaoka, Y., 1999. Generation of influenza A viruses entirely from cloned cDNAs. Proc. Natl. Acad. Sci. 96, 9345–9350.

Noda, T., Sagara, H., Yen, A., Takada, A., Kida, H., Cheng, R.H., Kawaoka, Y., 2006. Architecture of ribonucleoprotein complexes in influenza A virus particles. Nature 439, 490–492.

Noda, T., Sugita, Y., Aoyama, K., Hirase, A., Kawakami, E., Miyazawa, A., Sagara, H., Kawaoka, Y., 2012. Three-dimensional analysis of ribonucleoprotein complexes in influenza A virus. Nat. Commun. 3, 639.

Noda, T., Murakami, S., Nakatsu, S., Imai, H., Muramoto, Y., Shindo, K., Sagara, H., Kawaoka, Y., 2018. Importance of the 1+7 configuration of ribonucleoprotein complexes for influenza A virus genome packaging. Nat. Commun. 9, 1–10.

Ozawa, M., Maeda, J., Iwatsuki-Horimoto, K., Watanabe, S., Goto, H., Horimoto, T., Kawaoka, Y., 2009. Nucleotide sequence requirements at the 5′ end of the influenza A virus M RNA segment for efficient virus replication. J. Virol. 83, 3384–3388.

Paillart, J.C., Skripkin, E., Ehresmann, B., Ehresmann, C., Marquet, R., 1996. A loop-loop "kissing" complex is the essential part of the dimer linkage of genomic HIV-1 RNA. Proc. Natl. Acad. Sci. USA 93, 5572–5577.

Scheiffele, P., Roth, M.G., Simons, K., 1997. Interaction of influenza virus haemagglutinin with sphingolipid- cholesterol membrane domains via its transmembrane domain. EMBO J. 16, 5501–5508.

Schneider, C. a., Rasband, W.S., Eliceiri, K.W., 2012. NIH Image to ImageJ: 25 years of image analysis. Nat. Methods 9, 671–675.

Spitale, R.C., Crisalli, P., Flynn, R. a., Torre, E. a., Kool, E.T., Chang, H.Y., 2013. RNA SHAPE analysis in living cells. Nat. Chem. Biol. 9, 18–20.

Spronken, M.I., van de Sandt, C.E., de Jongh, E.P., Vuong, O., van der Vliet, S., Bestebroer, T.M., Olsthoorn, R.C.L., Rimmelzwaan, G.F., Fouchier, R.A.M., Gultyaev, A.P., 2017. A compensatory mutagenesis study of a conserved hairpin in the M gene segment of influenza A virus shows its role in virus replication. RNA Biol. 14, 1606–1616.

Takizawa, N., Watanabe, K., Nouno, K., Kobayashi, N., Nagata, K., 2006. Association of functional influenza viral proteins and RNAs with nuclear chromatin and sub-chromatin structure. Microbes Infect. 8, 823–833.

Takizawa, N., Kumakura, M., Takeuchi, K., Kobayashi, N., Nagata, K., 2010. Sorting of influenza A virus RNA genome segments after nuclear export. Virology 401, 248–256.

Takizawa, N., Momose, F., Morikawa, Y., Nomoto, A., 2016. Influenza A virus hemagglutinin is required for the assembly of viral components including bundled vRNPs at the lipid raft. Viruses 8, 249.

Williams, G.D., Townsend, D., Wylie, K.M., Kim, P.J., Amarasinghe, G.K., Kutluay, S.B., Boon, A.C.M., 2018. Nucleotide resolution mapping of influenza A virus nucleoprotein-RNA interactions reveals RNA features required for replication. Nat. Commun. 9, 465.

World Health Organization, 2011. Manual for the laboratory diagnosis and virological surveillance of influenza.

York, A., Hengrung, N., Vreede, F.T., Huiskonen, J.T., Fodor, E., 2013. Isolation and characterization of the positive-sense replicative intermediate of a negative-strand RNA virus. Proc. Natl. Acad. Sci. USA 110, E4238–E4245.

Zhao, L., Peng, Y., Zhou, K., Cao, M., Wang, J., Wang, X., Jiang, T., Deng, T., 2014. New insights into the nonconserved noncoding region of the subtype-determinant hemagglutinin and neuraminidase segments of influenza A viruses. J. Virol. 88, 11493–11503.